Progress In Electromagnetics Research C, Vol. 121, 49–63, 2022

Design and Analysis of Inscribed Fractal Super Wideband Antenna for Microwave Applications

Dipika Sagne* **and Rashmi A. Pandhare**

Abstract—This paper presents the design of a Super Wideband (SWB) antenna with enhanced bandwidth for microwave applications with a detailed parametric study of the methods used to enhance the bandwidth of the conventional antenna. The proposed SWB antenna has emerged from a traditional circular monopole antenna by experimenting with an inscribed fractal structure with a tapered feed line and partial ground plane with blended corners and achieved a super wideband frequency range from 2.31 GHz to 105.5 GHz with a fractional bandwidth of 192.1% and a Bandwidth Dimension Ratio (BDR) of 2154.88. The antenna has a relatively small electrical dimension, i.e., $0.33\lambda_0 \times 0.27\lambda_0$, where λ_0 corresponds to the lower-end operating frequency and exhibits good gain and efficiency characteristics. In order to observe the signal correlation of the proposed antenna, the time domain analysis using similar antennas in face-to-face and side-to-side scenarios has been performed using the EM simulation tool CST-STUDIO. The simulated gain varies from 1.28 to 9.35 dBi. The proposed antenna can be used for S, C, X, Ka, Ku, V, and W bands for microwave and millimetre wave applications. The simulated and measured results of the proposed antenna exhibit a good agreement.

1. INTRODUCTION

Compact and low-profile antennas are vital in high-performance aircraft, spacecraft, satellite, wireless communication, and missile applications where size, weight, cost, performance, ease of installation, and aerodynamic profile are constraints [1]. The recent developments in the field of modern communication need a wideband antenna for long-distance communication. Ultra-wideband (UWB) technology, with an operating frequency range of 3.1 GHz to 10.6 GHz allotted by the FCC, is able to provide a high data rate for modern wireless communication only for short distances due to its slow adaptation rate and long signal acquisition time, and thus limited to only indoor applications [2–6]. However, for outdoor communication, there is a high demand for a higher data rate and larger bandwidth for long-distance communication. Super wideband (SWB) antenna is a promising solution to the increased demand for connectivity, as it can be used for indoor as well as outdoor communication [5, 6]. SWB technology is more advantageous than narrow band technology. It can transmit data over long distances due to its wide bandwidth, and it also has advanced features such as increased channel capacity, improved time accuracy, and superior resolution [7]. According to the FCC [3, 6], an SWB antenna is one that can contribute to minimal levels on a decade bandwidth (10 : 1) for impedance bandwidth 10 dB return loss. SWB technology provides greater bandwidth and higher data rate, which can also be utilised to broadcast voice, video, and data at a faster rate. This technology is currently used in civil and military ranging and monitoring systems, and also used in Multichannel Multipoint Distribution Service (MMDS), WLAN, unlicensed UWB, vehicular radar, 5G, wireless network applications, satellite

Received 7 March 2022, Accepted 27 May 2022, Scheduled 27 June 2022
* Corresponding author: Dipika Sagne (deepika.sagne@gmail.com).
The authors are with the Department of Electronics & Communication Engineering, Indian Institute of Information Technology, Nagpur, India.

communication, microwave, and millimetre wave applications [5–9], and hence compressive works have been published on super wideband antennas.

An antenna consisting of a steering-shaped radiating patch with a tapered microstrip-fed circular ring with four elliptical spokes connecting to a central circular disc is reported in [6] for civilian and military wireless applications and achieves a percentage bandwidth of 175.2% with 2.3 GHz to 34.8 GHz and a gain of 4.76 dBi, but efficiency and gain vary with frequency. A modified bow-tie-shaped vertical patch is coupled with two symmetrical coplanar ground planes for wireless sensor node applications and is investigated in [8] with an operating band of 3.035 GHz–17.39 GHz (140.56%). It has been observed that efficiency and gain vary with frequency. In [9], a compact monopole SWB antenna consisting of an octagonal-ring shaped patch with a stub positioned on the top right corner with a notched partial ground plane has been presented for SWB applications. The designed antenna covers the frequency band from 2.59 GHz to 31.14 GHz with a percentage of 169% and a bandwidth ratio of 12.02 : 1. However, the gain is low and varies between 2 and 5 dBi.

A fractal antenna with a star structure inside a circular ring with a semi-elliptical ground plane for SWB applications with an impedance bandwidth of 4.6 GHz–52 GHz is presented in [10] with an average gain of 4 dBi in the measured frequency range as it varies over the frequency range. [11] describes a partially segmented circular monopole antenna with a notched elliptical partial ground plane which covers the frequency range from 0.96 GHz to 10.9 GHz with the percentage bandwidth of 167.22 with a low peak gain of 4 dBi for LTE2600, Wi-Fi, WLAN, and UWB applications. [12] proposes a skull shaped structure with a slotted rectangular partial ground plane design with a fractional bandwidth of 160.66% ranging from 3 GHz to 27.5 GHz and a peak gain of 6.3 dBi. In [13], a quasi-square with proper sizes and angles on the lower edges of the patch and ground plane with two circular slots is presented, which is a characteristic for SWB applications. The bandwidth is obtained from 3 GHz to 50 GHz with a variable gain of 1 to 9.47 dBi. A clover structured monopole antenna with a semi-elliptical "V" shaped slotted ground plane for SWB applications is presented in [14] with 176% bandwidth ranging from 1.9 to 30 GHz and gain varying from 0.7 to 5.6 dBi. [15] proposes a compact SWB trapezoid shape radiator with a semicircular ground and achieves impedance bandwidth from 1.42 GHz to 90 GHz with a maximum gain of 7.67 dB, but the cross-polar pattern is greater than that of the co-polar pattern, and time-domain analysis is also not investigated. In [16], a snowflake structure is achieved using a star-shaped fractal designed for 5G communication with an impedance bandwidth from 17.22 GHz to 180 GHz and an average gain of 6.4 dBi. However, simulation results are not verified with fabrication results. [17] describes a planar monopole antenna based on the hamming window function to provide 2.5 GHz to 110 GHz impedance bandwidth and reduced feed line width in order to improve the radiation pattern, though at higher frequencies, the reflection coefficient is degraded mostly due to the non-ideal frequency response.

In this paper, an exhaustive design and analysis of an inscribed fractal SWB antenna having a bandwidth ratio of 53.88 : 1 (192.1%) is investigated. The proposed antenna operates in a frequency range from 2.31 GHz to 105.5 GHz, and BDR of 2154.88. In this work, different methods to enhance the bandwidth are investigated and analysed. The design of the proposed antenna is derived from a printed circular monopole antenna as it gives a wide impedance bandwidth and omnidirectional radiation pattern. Initially, blended corners of the ground plane are used to improve the bandwidth up to some extent. Further, the fractal technique and tapered feed technique have been implemented to enhance the bandwidth of the proposed antenna. The proposed antenna is designed and investigated using the CST-EM software package in terms of the antenna's different parameters, including impedance bandwidth characteristics, radiation patterns, antenna gain, radiation efficiency, and group delay evaluation. Furthermore, the proposed antenna is fabricated, and results are measured using a vector network analyzer for microwave and millimetre wave applications.

2. ANTENNA CONFIGURATION

The configuration of the proposed SWB antenna is as shown in Fig. 1. The proposed antenna is fabricated on an RT Duroid ($\varepsilon_r = 2.2$, $\tan\delta = 0.0009$) substrate with thickness of 0.787 mm. The proposed antenna geometry consists of a circular radiating patch with radius 'r' along with the fractal geometry of two iterations. The 1st iteration consists of a circle with radius 'r_1' inscribed in a triangle

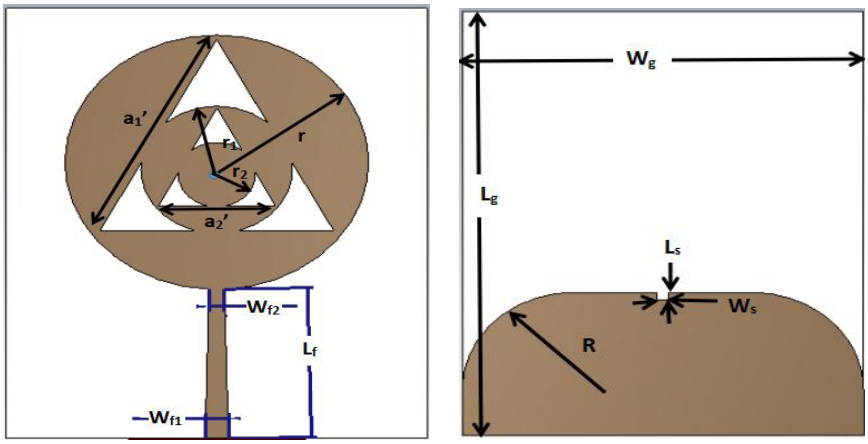

Figure 1. Configuration of proposed SWB antenna. (a) Front, (b) back view of an antenna.

with side length 'a_1'', and the 2nd iteration consists of radius 'r_2' inscribed in a triangle with side length a_2'. A tapered feed line is used with length L_f, width W_{f2} at the narrow end and W_{f1} at the other end in a top surface of the substrate as shown in Fig. 1(a). The blended partial ground plane with length L_{mg} and width W_g with a rectangular slot of $W_s \times L_s$ mm^2 dimensions at the ground plane of the substrate is shown in Fig. 1(b).

The design parameters of antenna mentioned in Table 1 are optimized using simulation with overall dimensions $44 \times 36 \times 0.787$ mm^3.

Table 1. Designed parameters of the proposed antenna.

Parameters	Dimensions (mm)	Parameters	Dimensions	Parameters	Dimensions
W_g	36	L_f	15.29	a_1	19.26
L_g	44	W_{f2}	1.3	a_1'	20.26
h	0.787	W_{f1}	2	r_1	6.49
r	13	W_s	1	a_2	9.12
L_{mg}	14.65	L_s	1	a_2'	10.12
p	0.64	R	10	r_2	3.24

The simulation result of this proposed antenna is shown in Fig. 2. It is observed that a good impedance matching has been achieved over the operating frequency band from 2.31 GHz to 105.06 GHz.

It has been observed that the proposed SWB antenna has a wide frequency range, enhanced bandwidth, with high BDR ratio despite the fact that the antenna is smaller in size which makes this antenna most suitable for various microwave applications. Different methods have been used in order to amend the conventional circular monopole antenna to a proposed high performance SWB antenna. The section below describes the stepwise process with all parametric studies of converting the basic conventional circular antenna to a modified fractal SWB antenna.

3. DESIGN AND ANALYSIS OF SWB ANTENNA

Initially, a conventional circular patch antenna with the full ground plane is designed as shown in Fig. 3(a) which resonates at 16.365 GHz with a bandwidth of 610 MHz. In order to enhance the impedance bandwidth monopole antennas are used [18–21], and hence the basic structure is further modified as shown in Fig. 3(b).

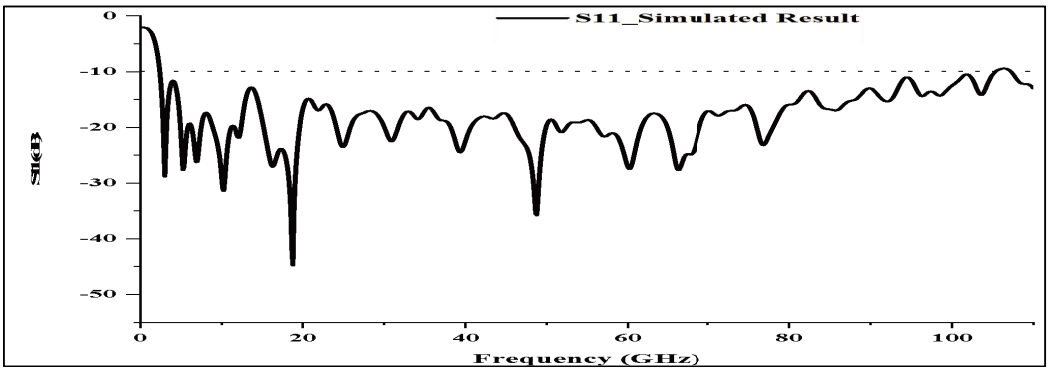

Figure 2. Simulation result for S parameter of proposed antenna.

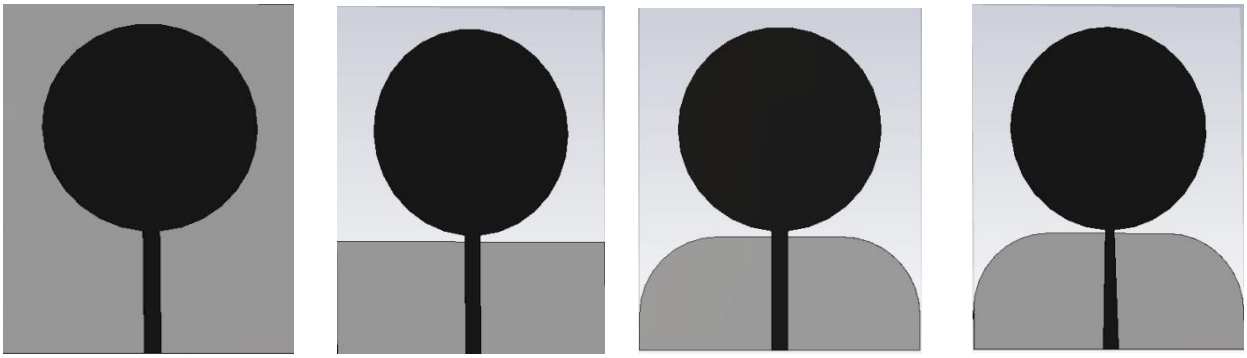

Figure 3. Stepwise design of a proposed antenna.

The outer circle radius of the monopole patch antenna is calculated for the lower edge frequency of 2.4 GHz using Eq. (1) as given below, where 'f_L' is the lower edge frequency, 'p' a gap between the ground plane and circular patch antenna, 'L_{mg}' the length of the ground plane, and 'r' the equivalent radius of a cylindrical monopole antenna [21].

$$f_L = \frac{7.2}{(L_{mg} + r + p)}\,\text{GHz} \tag{1}$$

The equivalent effective radius 'r_{eff}' is calculated using Eq. (2) [1] as given below, and the calculated equivalent radius of circular monopole antenna is equal to 13.30 mm.

$$r_{eff} = a\left[1 + \frac{2h}{\pi r \epsilon_r}\left[\ln\left(\frac{\pi r}{2h}\right) + 1.7726\right]\right] \tag{2}$$

To achieve the desired bandwidth and reflection coefficient below -10 dB, the length 'L_g' of the ground plane needs to be optimized. So, in order to enhance the bandwidth of circular monopole antenna, the effective length of the ground plane is optimized as shown in Table 2. The maximum bandwidth enhancement is obtained at 'L_{mg}' equal to 14.85 mm, which can also be observed by the length of the ground plane Vs. bandwidth graph.

The comparison of the simulated reflection coefficient at $L_{mg} = 14.85$ mm to the full ground plane is as shown in Fig. 4. It has been observed that the maximum bandwidth of 18.52 GHz is achieved by the partial ground technique, and hence, in comparison with the conventional circular patch antenna with full ground plane, a 98.85% enhancement in bandwidth has been observed.

This antenna covers a total bandwidth of 18.52 GHz, ranging from 2.31 GHz to 20.83 GHz, and the antenna is useful for S, C, X, and Ku band applications. However, to cover the other microwave

Table 2. Parametric analysis of variation of length of ground plane.

Length of Gnd Plane (mm)	Bandwidth (GHz)	Graph
3.5	0.41	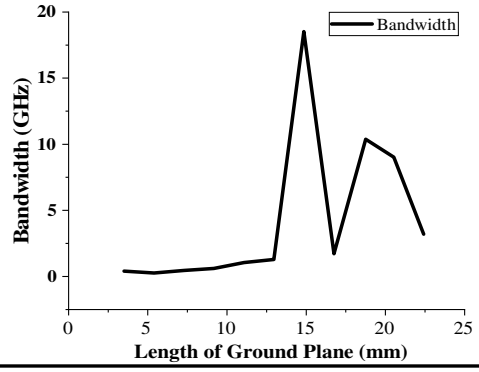
5.3	0.26	
7.28	0.463	
9.17	0.609	
11.07	1.05	
12.96	1.29	
14.85	18.52	
16.75	1.73	
18.75	10.38	
20.53	9.02	
22.42	3.2	

Table 3. Parametric analysis of blending of partial ground plane.

Blending Radius (mm)	Bandwidth (GHz)	Graph
2	19.65	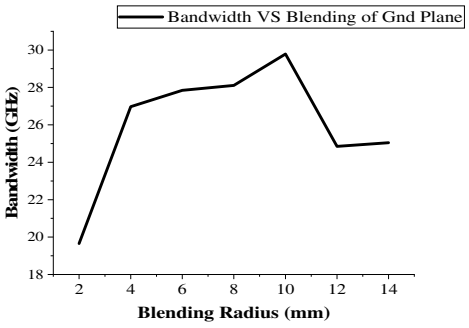
4	26.97	
6	27.84	
8	28.11	
10	29.781	
12	24.85	
14	25.04	

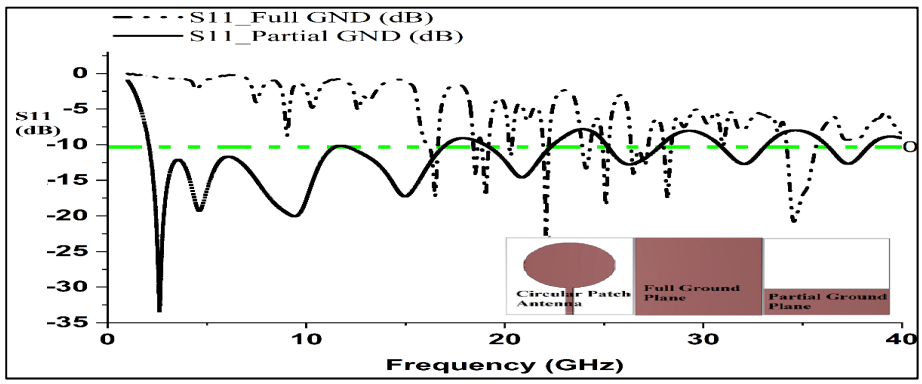

Figure 4. Bandwidth comparison for the partial and full ground plane.

applications, the bandwidth needs to be further improved and hence used blending to obtain linear phase characteristics of reflection coefficient [14] at the ground plane as shown in Fig. 3(c). Blending is introduced at the upper sharp edges of the partial ground plane of the proposed antenna. Table 3 shows the variation of bandwidth with respect to the blending radius 'R' and achieves the maximum

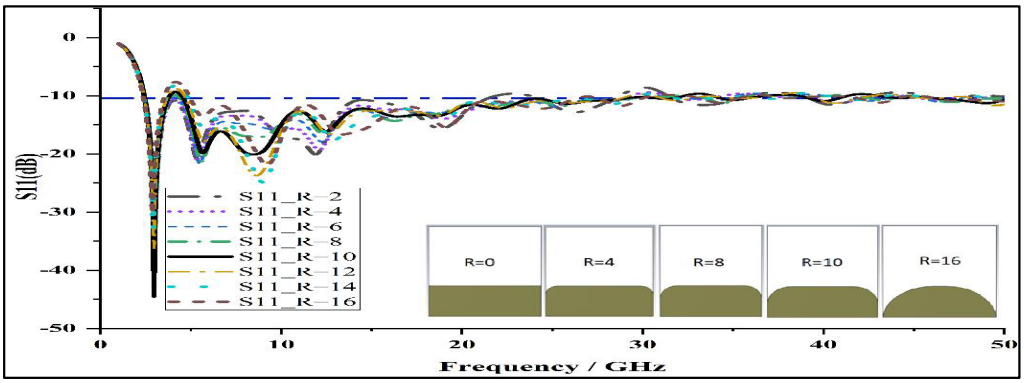

Figure 5. Parametric analysis results for blending of the ground plane.

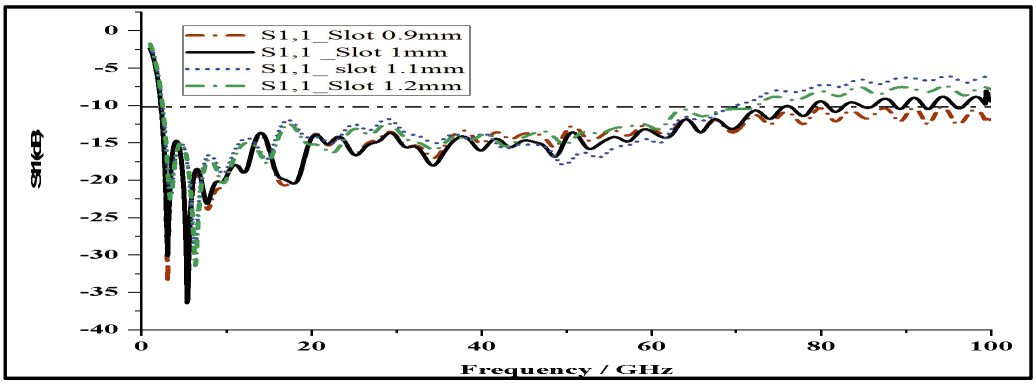

Figure 6. Comparison results of variation in slot dimensions.

bandwidth at $R = 10\,\text{mm}$, i.e., 29.781 GHz ranging from 2.31 GHz to 32.09 GHz. Fig. 5 shows the S_{11} results for different blending radii, and it has been observed that at $R = 10\,\text{mm}$ the bandwidth is increased by 37% as compared with the modified antenna with the partial ground plane.

Further, the feed line has been tapered near the antenna feeding point, which is connected to a $50\,\Omega$ SMA connector shown in Fig. 3(d) to improve the impedance matching at higher frequencies, which gives a wider impedance bandwidth [22]. An electromagnetic coupling exists between the patch and the partial ground plane. This effect is neutralized by introducing a slot or a notch on the partial ground plane as it increases an inductive effect. As a result, the antenna structure becomes resistive. So, the notch plays a very important role in enhancing impedance bandwidth, and it reduces the higher modes that appear at higher frequencies [23]. A slot with length L_s and width W_s is inserted in the partial ground plane with blended top corners as shown in Fig. 1(b), as it increases the electrical length of the patch antenna to concatenate the overall design. Fig. 6 depicts the result of a circular monopole antenna with a tapered feed line and the result of varying the slot dimensions. The optimized dimension of the slot is $1 \times 1\,\text{mm}^2$. However, as the slot dimensions increase, bandwidth is reduced as it reduces the higher modes at higher frequencies. It has been observed that the conventional circular antenna has been modified stepwise with all parametric studies and has obtained an impedance bandwidth up to 72.68 GHz.

4. DESIGN AND ANALYSIS OF FRACTAL SWB ANTENNA

The fractal geometry technique has been applied and investigated further in order to achieve the wideband behaviour of the modified circular monopole antenna and to enhance the performance of this antenna in terms of several factors such as gain, radiation pattern, directivity, return loss, and

bandwidth. The fractal geometry in planar antenna structures has been recognized as one of the most important techniques to improve the bandwidth. Fractal is a geometric shape consisting of self-similarity of the same structure and space-filling, which results in bandwidth enhancement and multiband, i.e., several resonant bands, and in combination, it can form an SWB antenna [24, 25]. The modified circular monopole antenna shown in Fig. 3(d) has an impedance bandwidth of 72.68 GHz ranging from 2.31 GHz to 74.99 GHz and is a further modified using fractal technique as shown in Fig. 6. The antenna in Fig. 3(d) shows the zeroth iteration or basic structure of the proposed fractal SWB antenna. The first iteration of fractal geometry is illustrated using Fig. 7(a) which shows the triangle inscribed in a circle, and Fig. 7(b) shows a circle with r_1 inscribed in an equilateral triangle with the length a_1.

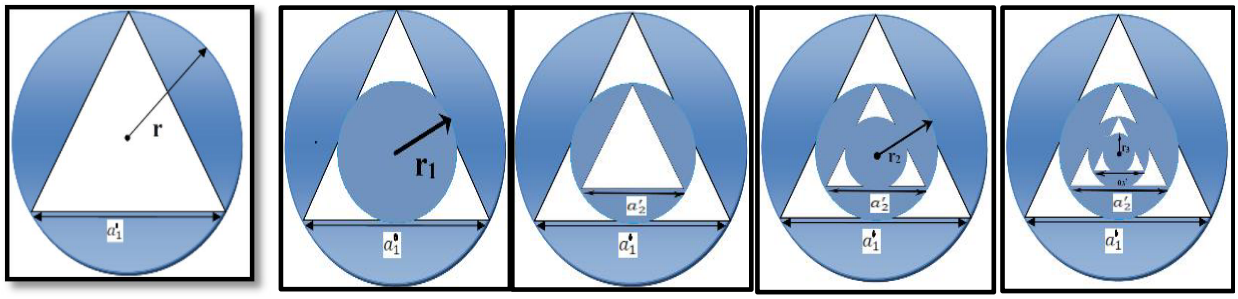

(a) (b) (c) (d) (e)

Figure 7. Fractal design steps of proposed antenna.

The parameters of the 1st iteration of fractal geometry are calculated using the following equation by applying trigonometry identity, i.e., triangle inscribed into the circle in Fig. 7(a), and the side length of an equilateral triangle is as follows:

$$a_1 = r * \sqrt{3} \tag{3}$$

In order to make conductivity and connectivity between the iterations of fractal geometry side length a_1 of the equilateral triangle is optimized by using Eq. (4), where 'a_1'' is the optimized length of an equilateral triangle which is calculated using optimized side length of equilateral triangle 'a_1', and 'r' is the radius of the circle.

$$a_1' = a_1 - \frac{a_1}{10} \tag{4}$$

By applying trigonometry identity to Fig. 7(b), i.e., circle inscribed into triangle, the radius of circle 'r_1' inscribed in a triangle is calculated using Eq. (5).

$$r_1 = \frac{a_1}{2\sqrt{3}} \tag{5}$$

Using similar techniques the side length of equilateral triangle 'a' and the radius of circle 'r' for the second and third iterations shown in Figs. 7(c)–(e) are calculated as follows:

$$a_n = r_{n-1} * \sqrt{3} \tag{6}$$

$$a_n' = a_n - \frac{a_n}{10} \tag{7}$$

$$r_n = \frac{a_n}{2\sqrt{3}} \tag{8}$$

From the above equations, it can be concluded that the derived equation for 'a_n' corresponds to the optimized side length of the equilateral triangle at the nth iteration, where 'r_n' is the radius at the nth iteration for fractal antenna. The values for 1st, 2nd, and 3rd iterations are calculated using above equation and mentioned in Table 1. Fig. 8 shows the comparison result of three iterative stages of fractal antenna. In the first iteration bandwidth is increased by 33% and in the second 37% as compared to without fractal. It has been observed that the 3rd iteration slightly reduces the bandwidth as compared 2nd iteration hence limit the antenna design up to 2nd iteration only.

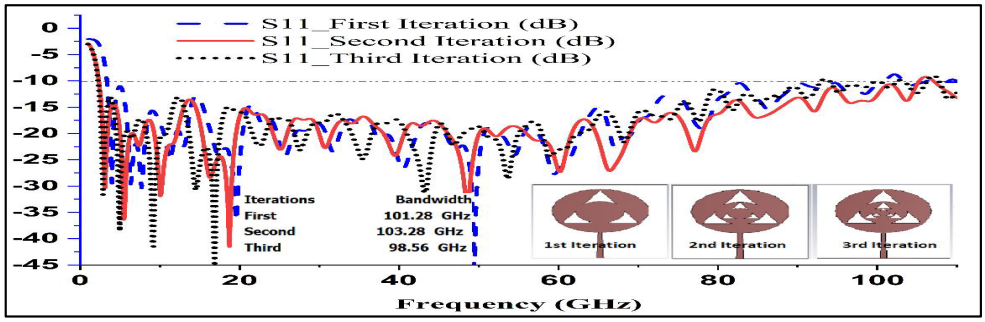

Figure 8. Parametric analysis of fractal iteration.

The proposed fractal SWB antenna provides 10 dB impedance bandwidth for the entire frequency spectrum of 2.31 GHz to 105.42 GHz with a fractional bandwidth 192% and BDR of 2154. The Bandwidth Dimension Ratio (BDR) is one of the important factors which specifies miniaturization and wide bandwidth, and it is calculated using the following equation [26].

$$\text{BDR} = \frac{\text{BW}\%}{\lambda_l * \lambda_w} \tag{9}$$

where λ_L and λ_W are the wavelengths associated with the lower cut of frequency f_L, and it is calculated using the following equation:

$$\lambda_l = \frac{L_g}{\lambda_0} \quad \text{and} \quad \lambda_w = \frac{W_g}{\lambda_0} \tag{10}$$

where W_g and L_g are the electrical width and length of the ground plane, respectively, and λ_0 is the cut of wavelength which is the ratio of speed of light 'c' and the lower edge frequency 'f_L'. Furthermore, in order to compare the proposed work with the available literature, the proposed SWB antenna has been compared in terms of electrical dimensions, percentage of bandwidth, BDR, bandwidth ratio, and peak gain with the few of the available SWB-based antennas in the literature, as shown in Table 4. From [6] and [8], it can be stated that though the bandwidth and BDR ratio of the referred antennas are greater than the designed antenna, the gain and bandwidth are less in the published work than

Table 4. Comparison of the proposed antenna with the antennas in the open literature survey.

Ref. No.	Electrical Dimensions	Frequency Range GHz	Bandwidth %	Bandwidth Ratio	BDR Ratio	Peak Gain dBi	Time response analysis
[6]	$0.27\lambda_0 \times 0.27\lambda_0 \times 0.012\lambda_0$	2.3–34.8	175	15.13 : 1	2403	4.76	No
[8]	$0.25\lambda_0 \times 0.20\lambda_0 \times 0.016\lambda_0$	3.035 to 17.39	140.56	5.72 : 1	2800	4.56	Yes
[9]	$0.34\lambda_0 \times 0.34\lambda_0 \times 0.0087\lambda_0$	2.59 to 31.14	169	12.02 : 1	1462	5	No
[10]	$0.29\lambda_0 \times 0.30\lambda_0 \times 0.024\lambda_0$	4.6 to 52	168	11.30 : 1	1903	4.6	No
[13]	$0.3\lambda_0 \times 0.3\lambda_0 \times 0.016\lambda_0$	3 to 50	188.5	16.6 : 1	2094	9.47	Yes
[14]	$0.32\lambda_0 \times 0.28\lambda_0 \times 0.0101\lambda_0$	1.9 to 30	176	15.78 : 1	1964	5.6	Yes
[16]	$1.16\lambda_0 \times 1.16\lambda_0 \times 0.045\lambda_0$	17.32 to 180	165	10.45 : 1	125.2	10.0	No
[17]	$0.33\lambda_0 \times 0.416\lambda_0 \times 0.0021\lambda_0$	2.5 to 110	191.1	37.93 : 1	1381	7.0	No
[22]	$0.09\lambda_0 \times 0.12\lambda_0 \times 0.0048\lambda_0$	0.9 to 100	196.4	111.1 : 1	1814	7.0	No
[25]	$0.32\lambda_0 \times 0.245\lambda_0 \times 0.020\lambda_0$	3.87 to 35	160.12	09.8 : 1	2083	8.5	Yes
[27]	$0.30\lambda_0 \times 0.35\lambda_0 \times 0.0074\lambda_0$	2.8 to 40	173.8	14.28 : 1	1904	5.5	Yes
[28]	$0.33\lambda_0 \times 0.33\lambda_0 \times 0.012\lambda_0$	2.31 to 40	188.56	34.63 : 1	1732	5.81	Yes
Proposed	$0.27\lambda_0 \times 0.33\lambda_0 \times 0.0060\lambda_0$	2.31 to 105.41	192	53.88 : 1	2154	9.35	Yes

the proposed SWB antenna that covers a larger band of frequency than the published work. However, from [9, 10, 13, 14, 16, 17, 25, 27, 28], it has been observed that the proposed SWB antenna has a wide frequency range, enhanced bandwidth, high peak gain, and high BDR ratio though the antenna is smaller in size than the referred SWB antenna. The superior performance of the proposed SWB antenna in terms of size, bandwidth, and gain makes the proposed antenna most suitable for various microwave applications.

5. FREQUENCY RESPONSE ANALYSIS

In frequency domain analysis, simulated results of the proposed SWB antenna are analysed to elaborate reflection coefficient, co- and cross-polarizations, gain, efficiency, and surface current. Fig. 2 shows the S_{11} parameter for the proposed SWB antenna with an operating range of 2.31 GHz to 105.06 GHz with reasonable impedance matching all over the spectrum. Fig. 9 shows the simulated co- and cross-polarization radiation patterns of the proposed SWB antenna for 2.4 GHz, 5 GHz, 15 GHz, 40 GHz, 60 GHz, and 100 GHz, respectively, where at 2.4 GHz and 5.5 GHz it shows an omnidirectional radiation pattern with gains of 1.54 dBi and 3.79 dBi. The theta 'Θ' and phi 'Φ' are spherical coordinates to the Cartesian axis, where 'Θ' varied from 0 to 360 degrees, and 'Φ' varied from 0 and 90 degrees for co- and cross-polarizations in the E-plane, i.e., y-z plane, and 90 and 0 degrees for co- and cross-polarizations in the H-plane, i.e., x-z plane. At lower frequencies it shows an omnidirectional radiation pattern. From 20 GHz, the radiation pattern is disturbed due to a change in the area of radiation and current distribution, i.e., nonuniform. The cross-polarization, i.e., unwanted radiation, is less at lower frequencies but increases in some respects at higher frequencies, as shown in Fig. 9.

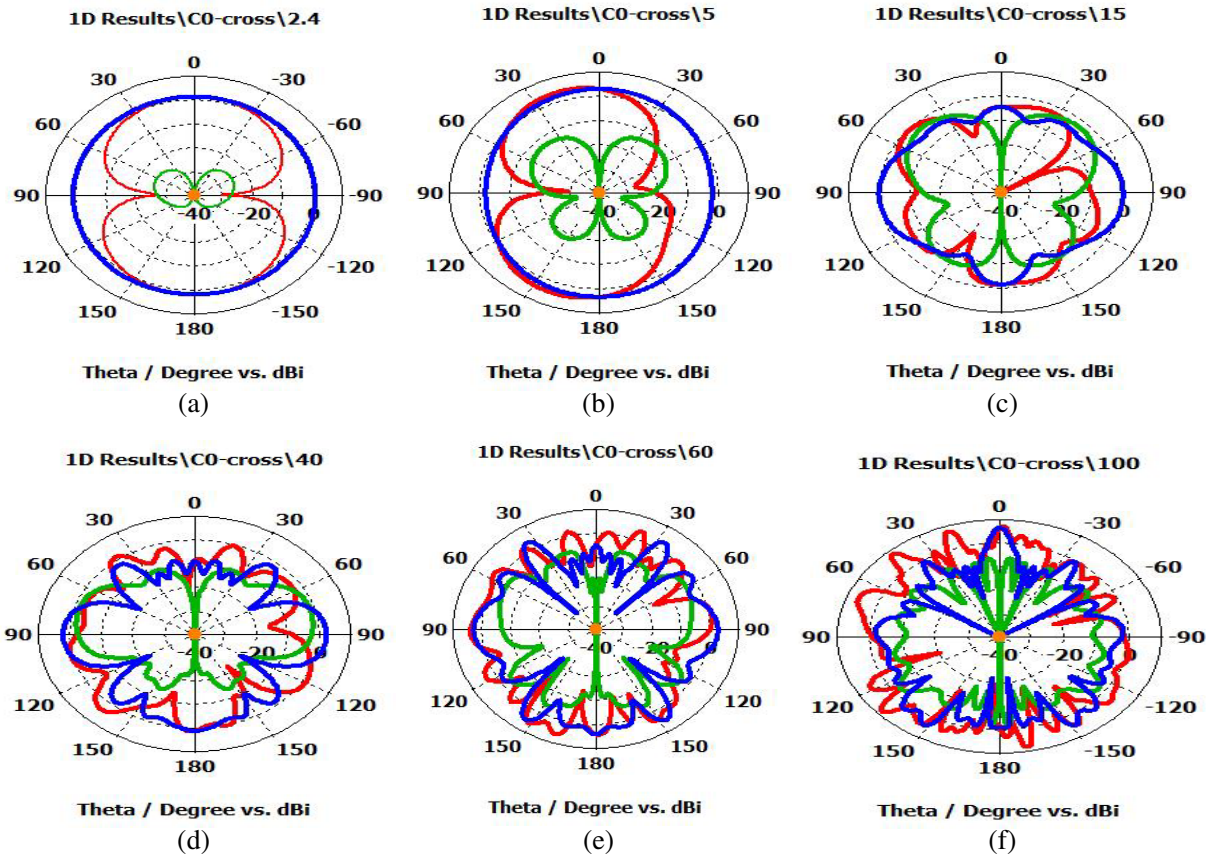

Figure 9. 2D radiation pattern for designed antenna at different frequencies. (a) 2.4 GHz, (b) 5 GHz, (c) 15 GHz, (d) 40 GHz, (e) 60 GHz, (f) 100 GHz.

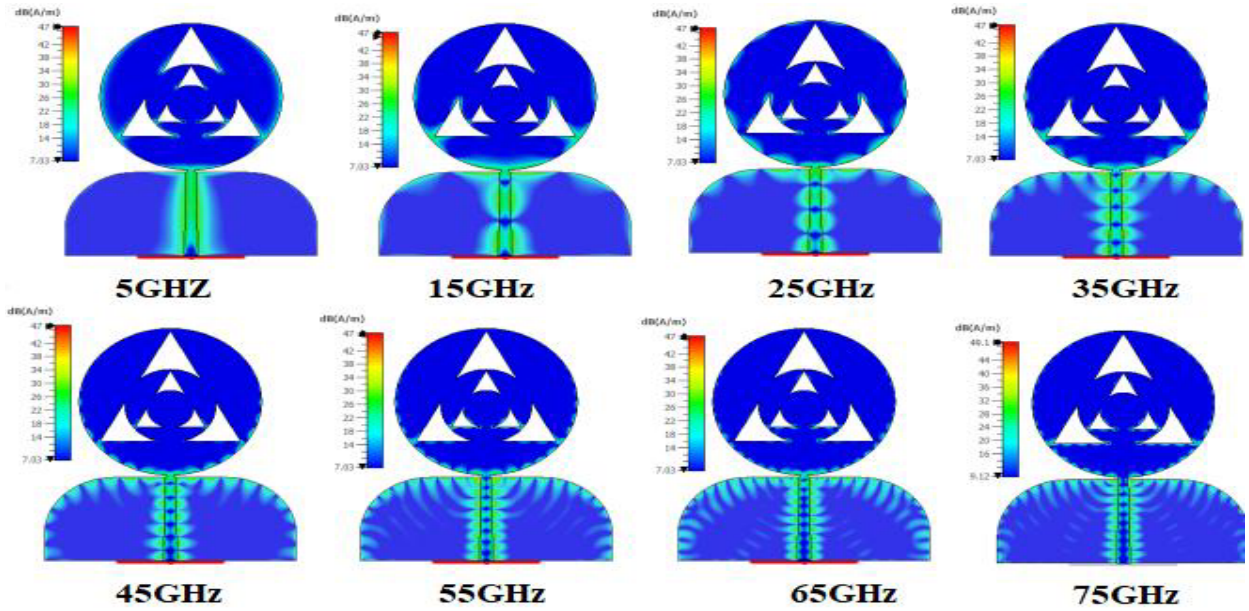

Figure 10. Surface current distribution of proposed antenna with various resonance mode.

However, at higher frequencies, higher operating modes appear, so radiated power is also distributed on other sides of the antenna, hence the overall pattern is disturbed. Eventually, radiated power on the front and back of the proposed SWB antenna is reduced to low radiation in the front and back lobes because this antenna will inhibit deviated omnidirectional pattern [29].

The designed SWB antenna's surface current distribution is shown in Fig. 10, corresponding to frequencies of 5 GHz, 15 GHz, 25 GHz, 35 GHz, 45 GHz, 55 GHz, 65 GHz, and 75 GHz, respectively. Current concentration in lower half of patch antenna indicates that the number of modes kicks in, for 5 GHz frequency single donut shaped radiation pattern near the feed line indicating omnidirectional radiation pattern. As frequency increases, the number of modes increases as shown in Fig. 10, and the radiation pattern is disturbed to some extent as shown in Fig. 11.

Figure 11 shows the efficiency vs. frequency graph, where the total efficiency varies from 0.87 to 0.99, and Fig. 12 shows the impedance of the antenna with average value of $55.82 - j0.0048\,\Omega$.

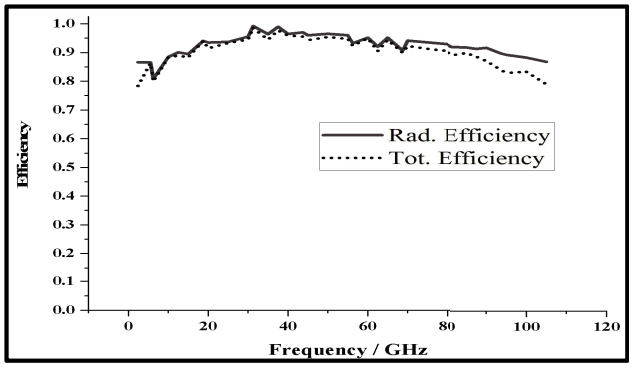

Figure 11. Efficiency vs frequency graph.

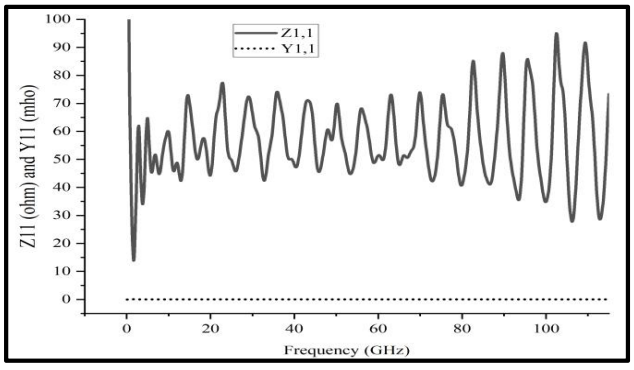

Figure 12. Impedance vs frequency graph.

6. TIME RESPONSE ANALYSIS

In order to analyse the time domain response, the fidelity factor plays a vital role in minimising the distortion in the modulated signal. The time domain analysis for the proposed fractal monopole antenna

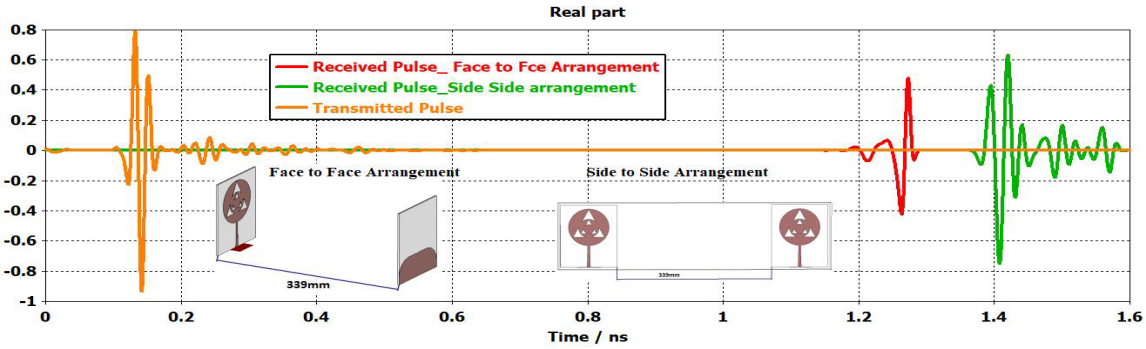

Figure 13. Transmit and receive signal for face to face and side to side arrangement.

is performed in the face-to-face and side-to-side alignments by placing the same type of two antennas 339 mm apart from each other, i.e., the minimum required far field distance [30] shown in Fig. 13. To validate the proposed SWB antenna, time domain analysis is performed by transmitting short-duration pulses of a few hundred picoseconds and obtaining a clone of the transmitted pulse [26]. Due to signal distortion, transmitter and receiver pulses are not the same, but the receiver antenna must recognize the pulses sent by the transmitter antenna. Thus, time domain analysis plays an important role in finding the signal distortion [12]. In the fidelity factor, the difference between Tx and Rx pulses can be investigated using the arrangement shown in Fig. 8. Normalization of Tx and Rx pulses is performed using Eqs. (11) and (12) [31].

$$T_s^n = \frac{T_s(t)}{\sqrt{\int_{-\infty}^{\infty} |T_s(t)|^2 \, dt}} \tag{11}$$

$$R_s^n = \frac{R_s(t)}{\sqrt{\int_{-\infty}^{\infty} |R_s(t)|^2 \, dt}} \tag{12}$$

where T_s^n is recognized as the normalized Tx pulse, and R_s^n is recognized as the normalized Rx pulse. The amplitude of the Rx pulse is less than the Tx pulse, so the normalization has been performed only to find similarity between the wave shapes of the pulses. The fidelity factor equation is calculated using point to point cross correlation between the normalized pulses as follows: Eq. (13) [31].

$$FF = \max \int_{-\infty}^{\infty} T_s^n(t) \, R_s^n(t) \, (t+\tau) dt \tag{13}$$

However, group delay of the system has been observed for both face-to-face and side-to-side arrangement, as shown in Fig. 14. The group delay is observed between 1.23 and 1.27 ns, which is almost constant and indicates the non-dispersive nature of the proposed antenna, whereas the value of the group delay is acceptable up to 3.8 ns [31]. Group delay is calculated using Eq. (14), whereas $d\emptyset$ is the phase of transmission coefficient (S_{21}).

$$\text{Group Delay} = -\frac{d\emptyset}{dw} \tag{14}$$

7. MEASUREMENT TEST SETUP & RESULTS DISCUSSION

The proposed antenna has been modelled and designed using 3D Electromagnetic Software; CST (Computer Simulation Technology) based on Finite Integration Technique (FIT) and then fabricated on RT Duroid material as shown in Fig. 15 and Fig. 16 representing the measurement test setup of fabricated prototype antenna.

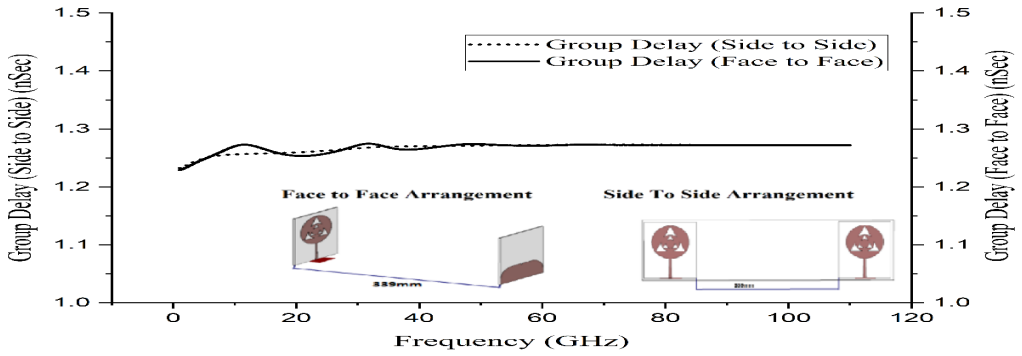

Figure 14. Group delay for face to face and side to side arrangement.

Figure 15. Front and back side of fabricated patch antenna.

Figure 16. Measurement set up of proposed antenna in anechoic chamber.

7.1. Reflection Coefficient (S_{11}) Characteristics

The performance was evaluated for the optimized parameters of the fabricated antenna. Fig. 17 shows the comparison result of the S_{11} parameter between simulated and measured results with permissible deviation.

The measured result for the S_{11} parameter has good agreement with the simulated response, and S_{11} is below 10 dB in the entire range. The slight difference that occurs is due to the fabrication tolerance.

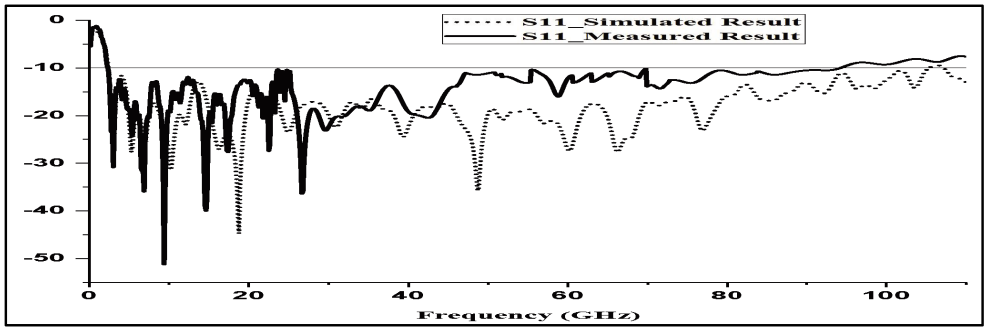

Figure 17. Comparison of simulated and fabricated results of frequency vs S_{11} (dB).

7.2. Peak Gain

Figure 18 shows the comparisons of measured and simulated gain results. It has been done by placing two identical antennas face-to-face and using Frii's power transmission equation [32]. The simulated gain permissible deviation is followed by the measured gain. The gain varies from 1.23 to 9.35 dBi and is nearly constant over the frequency range of 20 GHz to 75 GHz, i.e., between 6 and 7 dBi. It can be observed that there is a close agreement between simulated and measured results.

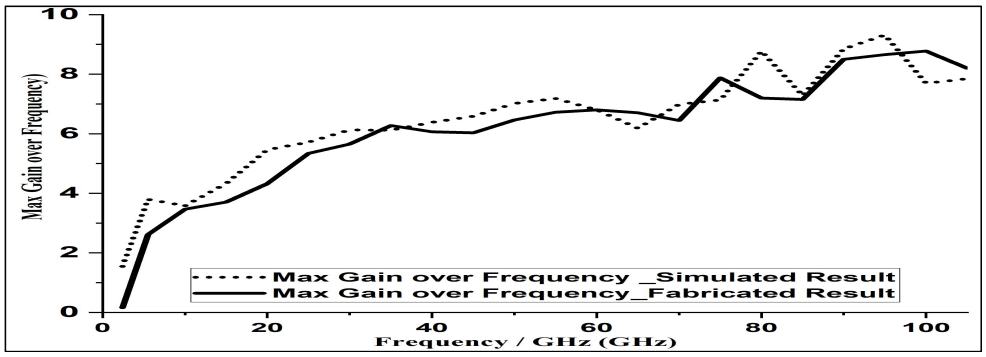

Figure 18. Comparison of simulated and measured result for gain measurement.

8. CONCLUSION

In this work, a circle-shaped inscribed fractal SWB antenna with a slotted partial ground plane is presented for microwave and millimetre wave applications. The proposed SWB antenna has a wider impedance bandwidth (2.31 GHz to 105.5 GHz), higher gain, and better radiation efficiency than previously described structures in the literature. The time domain analysis has also been performed, and the group delay is observed between 1.23 and 1.27 ns, which is almost constant with variation less than 0.1 ns over the entire frequency band without notch bands. Minimal distortion and less variation in the transmitted signal accomplish the requirements of SWB communication systems. The prototype model of the proposed SWB antenna was fabricated, and an overall good agreement was observed between simulated and experimental results, which makes the proposed antenna suitable for medical diagnostic imaging applications, Global Positioning System (GPS), airborne radar applications, satellite communication, and vehicular radar systems.

REFERENCES

1. Balanis, C. A., *Antenna Theory: Analysis and Design*, John Wiley & Sons, 2015.
2. Balani, W., et al., "Design techniques of super-wideband antenna — Existing and future prospective," *IEEE Access*, Vol. 7, 141241–141257, 2019.
3. "Revision of Part 15 of the Commission's rules regarding ultra wideband transmission systems," 2002.
4. Ali, T., B. K. Subhash, S. Pathan, and R. C. Biradar, "A compact decagonal-shaped UWB monopole planar antenna with truncated ground plane," *Microwave and Optical Technology Letters*, Vol. 60, No. 12, 2937–2944, Dec. 2018, doi: 10.1002/mop.31448.
5. Dhasarathan, V., M. Sharma, M. Kapil, P. C. Vashist, S. K. Patel, and T. K. Nguyen, "Integrated bluetooth/LTE2600 superwideband monopole antenna with triple notched (WiMAX/WLAN/DSS) band characteristics for UWB/X/Ku band wireless network applications," *Wireless Networks*, Vol. 26, No. 4, 2845–2855, May 2020, doi: 10.1007/s11276-019-02230-0.
6. Alluri, S. and N. Rangaswamy, "Compact high bandwidth dimension ratio steering-shaped super wideband antenna for future wireless communication applications," *Microwave and Optical Technology Letters*, Vol. 62, No. 12, 3985–3991, Dec. 2020, doi: 10.1002/mop.32541.
7. Dey, S. and N. C. Karmakar, "Design of novel super wide band antenna close to the fundamental dimension limit theory," *Scientific Reports*, Vol. 10, No. 1, 16306, Dec. 2020, doi: 10.1038/s41598-020-73478-2.
8. Azim, R., M. T. Islam, H. Arshad, Md. M. Alam, N. Sobahi, and A. I. Khan, "CPW-fed super-wideband antenna with modified vertical bow-tie-shaped patch for wireless sensor networks," *IEEE Access*, Vol. 9, 5343–5353, 2021, doi: 10.1109/ACCESS.2020.3048052.
9. Okan, T., "A compact octagonal-ring monopole antenna for super wideband applications," *Microwave and Optical Technology Letters*, Vol. 62, No. 3, 1237–1244, Mar. 2020, doi: 10.1002/mop.32117.
10. Singhal, S. and A. K. Singh, "Modified star-star fractal (MSSF) super-wideband antenna," *Microwave and Optical Technology Letters*, Vol. 59, No. 3, 624–630, Mar. 2017, doi: 10.1002/mop.30357.
11. Okas, P., A. Sharma, G. Das, and R. K. Gangwar, "Elliptical slot loaded partially segmented circular monopole antenna for super wideband application," *AEU — International Journal of Electronics and Communications*, Vol. 88, 63–69, May 2018, doi: 10.1016/j.aeue.2018.03.004.
12. Rahman, M. A., M. S. J. Singh, M. Samsuzzaman, and M. T. Islam, "A compact skull-shaped defected ground super wideband microstrip monopole antenna for short-distance wireless communication," *International Journal of Communication Systems*, Vol. 33, No. 14, e4527, Sep. 2020, doi: 10.1002/dac.4527.
13. Oskouei, H. R. D., A. R. Dastkhosh, A. Mirtaheri, and M. Naseh, "A small cost-effective super ultra-wideband microstrip antenna with variable band-notch filtering and improved radiation pattern with 5G/IoT applications," *Progress In Electromagnetics Research M*, Vol. 83, 191–202, 2019.
14. Palaniswamy, S. K., M. Kanagasabai, S. Arun Kumar, M. G. N. Alsath, S. Velan, and J. K. Pakkathillam, "Super wideband printed monopole antenna for ultra wideband applications," *International Journal of Microwave and Wireless Technologies*, Vol. 9, No. 1, 133–141, Feb. 2017, doi: 10.1017/S1759078715000951.
15. Rahman, S. U., Q. Cao, H. Ullah, and H. Khalil, "Compact design of trapezoid shape monopoleantenna for SWB application," *Microwave and Optical Technology Letters*, Vol. 61, No. 8, 1931–1937, Aug. 2019, doi: 10.1002/mop.31805.
16. Malik, R., P. Singh, H. Ali, and T. Goel, "A star shaped superwide band fractal antenna for 5G applications," *2018 3rd International Conference for Convergence in Technology (I2CT)*, 2018, doi: 10.1109/I2CT.2018.8529404.
17. Seyfollahi, A. and J. Bornemann, "Printed-circuit monopole antenna for super-wideband applications," *European Conference on Antennas & Propagation*, 2018.

18. Manohar, M., R. S. Kshetrimayum, and A. K. Gogoi, "Printed monopole antenna with tapered feedline, feed region and patch for super wideband applications," *IET Microwaves, Antennas & Propagation*, Vol. 8, No. 1, 39–45, Jan. 2014, doi: 10.1049/iet-map.2013.0094.
19. Ray, K. P. and S. Tiwari, "Ultra wideband printed hexagonal monopole antennas," *IET Microwaves, Antennas & Propagation*, Vol. 4, No. 4, 437, 2010, doi: 10.1049/iet-map.2008.0201.
20. Kundu, S., "Experimental study of a printed ultra-wideband modified circular monopole antenna," *Microwave and Optical Technology Letters*, Vol. 61, No. 5, 1388–1393, May 2019.
21. Ray, K. P. and Y. Ranga, "Ultrawideband printed elliptical monopole antennas," *IEEE Transactions on Antennas and Propagation*, Vol. 55, No. 4, 1189–1192, Apr. 2007, doi: 10.1109/TAP.2007.893408.
22. Manohar, M., R. S. Kshetrimayum, and A. K. Gogoi, "Super wideband antenna with single band suppression," *International Journal of Microwave and Wireless Technologies*, Vol. 9, No. 1, 143–150, Feb. 2017, doi: 10.1017/S1759078715000963.
23. Balani, W., M. Sarvagya, A. Samasgikar, T. Ali, and P. Kumar, "Design and analysis of super wideband antenna for microwave applications," *Sensors*, Vol. 21, No. 2, 477, Jan. 2021, doi: 10.3390/s21020477.
24. Das, S., D. Mitra, and S. R. Bhadra Chaudhuri, "Staircase fractal loaded microstrip patch antenna for super wide band operation," *Progress In Electromagnetics Research C*, Vol. 95, 183–194, 2019.
25. Singhal, S., "Asymmetrically fed octagonal Sierpinski band-notched super-wideband antenna," *Journal of Computational Electronics*, Vol. 16, No. 1, 210–219, Mar. 2017, doi: 10.1007/s10825-016-0948-5.
26. Mao, S.-G., J.-C. Yeh, and S.-L. Chen, "Ultrawideband circularly polarized spiral antenna using integrated balun with application to time-domain target detection," *IEEE Transactions on Antennas and Propagation*, Vol. 57, No. 7, 1914–1920, Jul. 2009.
27. Kundu, S. and A. Chatterjee, "A compact super wideband antenna with stable and improved radiation using super wideband frequency selective surface," *AEU — International Journal of Electronics and Communications*, Vol. 150, 154200, Jun. 2022, doi: 10.1016/j.aeue.2022.154200.
28. Sharma, V., Gunaram, J. K. Deegwal, and D. Mathur, "Super-wideband compact offset elliptical ring patch antenna for 5G applications," *Wireless Personal Communications*, Vol. 122, No. 2, 2022, doi: 10.1007/s11277-021-08965-4.
29. Dey, S., M. S. Arefin, and N. C. Karmakar, "Design and experimental analysis of a novel compact and flexible super wide band antenna for 5G," *IEEE Access*, Vol. 9, 46698–46708, 2021, doi: 10.1109/ACCESS.2021.3068082.
30. Singh, S., R. Varma, M. Sharma, and S. Hussain, "Superwideband monopole reconfigurable antenna with triple notched band characteristics for numerous applications in wireless system," *Wireless Personal Communications*, Vol. 106, No. 3, 987–999, Jun. 2019, doi: 10.1007/s11277-019-06199-z.
31. Tang, M.-C., R. W. Ziolkowski, and S. Xiao, "Compact hyper-band printed slot antenna with stable radiation properties," *IEEE Transactions on Antennas and Propagation*, Vol. 62, No. 6, 2962–2969, Jun. 2014, doi: 10.1109/TAP.2014.2314299.
32. Haraz, O. M., A.-R. Sebak, and S. A. Alshebeili, "Design of a printed log-periodic dipole array antenna with high gain for millimeter-wave applications," *International Journal of RF and Microwave Computer-Aided Engineering*, Vol. 25, No. 3, 185–193, Mar. 2015, doi: 10.1002/mmce.20848.